Journal of Magnetic Resonance 303 (2019) 67–74

Contents lists available at ScienceDirect

Journal of Magnetic Resonance

journal homepage: www.elsevier.com/locate/jmr

A novel pulse sequence and inversion algorithm of three-dimensional low field NMR technique in unconventional resources

Jianyu Liu, Yiren Fan *, Tingcong Qiu, Xinmin Ge, Shaogui Deng, Donghui Xing

School of Geosciences in China University of Petroleum, Qingdao 266580, PR China
Laboratory for Marine Mineral Resources, Qingdao National Laboratory for Marine Science and Technology, Qingdao 266071, PR China

ARTICLE INFO

Article history:
Received 4 March 2019
Revised 9 April 2019
Accepted 10 April 2019
Available online 11 April 2019

Keywords:
Inverse theory
Joint inversion
Numerical modeling
NMR
Pulse sequence

ABSTRACT

Compared with two-dimensional (2D) nuclear magnetic resonance (NMR) technique like correlations among the transversal relaxation time (T_2), the longitudinal relaxation time (T_1), and the diffusion coefficient correlation (D), three-dimensional (3D) NMR technique is superior with the complete measurement of T_2, T_1, and D simultaneously. It can solve the problem of overlaps in 2D correlation map and is helpful to characterize relaxation components in unconventional resources such as tight gas and oil shale. However, the existed 3D NMR technique is restricted due to the loss of short relaxation information and the inversion inaccuracy that caused by the incomplete measurement of the diffusion editing window. We developed a tri-window pulse sequence to collect the full decaying information of porous media. In the first window, the inversion-recovery pulse sequence is applied for T_1 encoding. In the second window, D and T_2 are encoded by an adjustable continuous pulse field gradient and echo spacing (TE). In the last window, CPMG with the shortest TE is used to acquire diffusion-free relaxation information. We then proposed a joint inversion algorithm named "composite-data-processing" to obtain the 3D correlation map. The algorithm adopts the dimension reduction technique and the truncated singular value decomposition (TSVD) to speed up the inversion process and enhance the inversion stability. Numerical simulations show that good estimations of the inversion results are obtained at different signal to noise ratios (SNRs). Our results suggest that the novel pulse sequence and inversion algorithm of 3D NMR can be effectively applied to the exploration of unconventional resources.

1. Introduction

Low field nuclear magnetic resonance (NMR) acts as an important technique in well logging and core analysis [1,2]. All NMR signals come from the hydrogen nuclei in fluid in the pore space, while the matrix does not contribute to the signal. Multiple petrophysical parameters such as transverse relaxation time (T_2), longitudinal relaxation time (T_1), and diffusion coefficient (D) can be obtained and provide lithology-independent porosity, saturation, pore size distribution, as well as permeability.

One-dimensional (1D) and 2D NMR have achieved good application in conventional resources. 1D NMR are recorded independently either in terms of T_1 or T_2 based on inversion recovery (IR), saturation recovery (SR) or Carr–Purcell–Meiboom–Gill (CPMG) pulse sequence. 2D NMR utilizes IR-CPMG, SR-CPMG, drive equilibrium (DE) to obtain T_1-T_2 or T_1/T_2-T_2 spectrum [3–6]. Pulsed filed gradient (PFG) is the most common diffusion encoding method used for T_2-D NMR, and BP-PFG (Bi-polar pulsed filed gradient), MSE-PFG (Multi-spin echo pulsed filed gradient), LED-PFG (Longitudinal eddy decay pulsed filed gradient) and DMSE-PFG (Double multi-spin echo pulsed filed gradient) are proposed for special purposes [7–14]. In addition, a suite of CPMG measurements with varying echo spacings (TE) in constant magnetic field gradients, diffusion editing pulse sequence (CPMG-DE) and modified CPMG pulse sequence can also be used to generate T_2-D or T_2-G spectrum [15–18]. NMR spectrums are obtained from magnetization decay data and the inversion problem can be reduced to the first kind of Fredholm integral equation which is ill-conditioned in the sense that small noise in the data can cause significant changes in the resulting spectrum [19]. Common methods presented to solve ill-posed inverse Laplace transform problem are iterative and regularized algorithms such as uniform-penalty (UPEN) [20], Butter-Reeds-Dawson (BRD) [21], truncated singular value decomposition (TSVD) [22], simultaneous iterative

* Corresponding author at: School of Geosciences in China University of Petroleum, Qingdao 266580, PR China.
E-mail address: fanyiren@upc.edu.cn (Y. Fan).

https://doi.org/10.1016/j.jmr.2019.04.009
1090-7807/

reconstruction technique (SIRT) [23], non-negative least squares (NNLS) [24], and intelligent optimization algorithms such as genetic algorithm [25], simulated annealing (SA) [26], differential evolution (DE) [27], Monte Carlo (MC) [28] and Lloyd-Max optimal quantization [29]. In addition to the above methods used in 1D NMR inversion, common methods of inverting 2D NMR data is transforming the 2D inversion problem into an equivalent 1D inversion problem using Kronecker products. Based on this theory, the data process of 2D NMR inversion can be decomposed to three steps: data compression, dimension reduction and inversion [30–38].

However, many restrictions obstruct the application of 1D and 2D NMR, especially in the unconventional reservoirs and cores, which contain so many complex relaxation components that 2D NMR experiments fail to acquire, process and interpret data accurately. In addition, fluid viscosity, wettability, pore structure and other influence factors lead to the overlapping of various components in 2D spectrums and difficulties in interpretation [39–42]. Thus, the study of 3D NMR has been carried out gradually both in data acquisition [43], processing [44–49] and interpretation [50–52]. The common 3D pulse sequence may have considerable results for conventional cores or reservoirs such as sandstone or carbonate. However, we obtained the unsatisfactory results when we implemented these methods to the unconventional cores or reservoirs such as shale, heavy oil reservoir, tight sandstone and bituminous sandstone, in which many complex relaxation components have a wide range of T_1, T_2 and D, such as crystal water, clay bound water, capillary bound water, free water, light hydrocarbon, heavy hydrocarbon, kerogen, and bitumen. Generally speaking, insufficient information on complex relaxation components and untargeted inversion algorithm lead to these unsatisfied results. Therefore, a lot of improvement is required in 3D NMR technology in data acquisition and inversion method.

This paper is organized as follows. In Section 2, we systematically elaborate the statement of the problem in 3D NMR, including data format and equation for different encode methods. In Section 3, we introduce a new 3D pulse sequence to collect decay data and a joint inversion scheme to recover the complicate components. In Section 4, we carry out numerical simulations by a tight oil shale model to validate the new method. Finally, we show the conclusion and discussion in the last section.

2. Statement of the problem

Although there are many types of pulse sequence based on different encode methods, the measured magnetization of a porous sample can be expressed as following according to the NMR relaxation mechanism

$$b(t,TE,Tw,G)=\iiint f(T_1,T_2,D)k_1(Tw,T_1)k_2(t,T_2)k_3 \times(t,TE,G,D)dDdT_1dT_2+\varepsilon \quad (1)$$

where $b(t,TE,Tw,G)$ is the amplitude of the spin echo train at detection time t, which characterizes the evocation of the magnetization of the spin echo, $f(T_1,T_2,D)$ is the 3D proton density distribution function, $k_1(Tw,T_1)$, $k_2(t,T_2)$ and $k_3(t,TE,G,D)$ are the kernel functions of T_1, T_2 and D respectively, ε is noise term, which is usually assumed to be additive, white and Gaussian. The aim of our work is to calculate $f(T_1,T_2,D)$ from the measured $b(t,TE,Tw,G)$ by 3D inverse Laplace transformation.

The evolution of NMR signal is dependent on kernel functions, which are determined by pulse sequence and acquisition parameters. Apparently, data format should be taken into account in pulse sequence design and inversion algorithm study.

The most widely used pulse sequence for T_1 encoding in multi-dimensional NMR are IR and SR, where the kernel functions can be expressed as

$$k_1(T_W,T_1)=1-\alpha\exp(-T_W/T_1) \quad (2)$$

Note that α is polarization factor. $\alpha=1$ for SR and $\alpha=2$ for IR respectively. Tw denotes the wait time, the time between the end of a pulse sequence and the start of the next pulse sequence excitation.

According to the principle of CPMG pulse sequence, the kernel function K_2 referred to diffusion-free relaxation can be expressed as

$$k_2(t,T_2)=\exp(-t/T_2) \quad (3)$$

The kernel function K_3 referred to diffusion relaxation has different expressions according to the diffusion editing methods. Some types of K_3 are separate while some are tangled with K_2. Therefore, we list four most widely used T_1-T_2-D pulse sequences (Fig. 1) and analyze K_3 respectively. (a) is the regular CPMG pulse sequence, in which T_1, T_2 and D are encoded by IR or SR pulse sequence with varying TW and CPMG with varying TE. (b) is the tri-window pulse sequence based on IR or SR and modified CPMG. The second window has a fixed width of t_0, where echo spacing (TE_1) varies from the smallest to the largest value allowed and the diffusion effect is encoded in the initial amplitude of spin echo in the third window. T_2 is encoded in the third window using the regular CPMG with the smallest TE to minimize the diffusion effect. (c) is the 3D pulse sequence based on IR or SR and CPMG-DE. In this case, the independent variable which encodes diffusion information is the echo spacing (TE_1) in the second window and there are only two spin echoes. The increase of TE_1 decreases the amplitude of subsequent echoes due to diffusion effects. The remaining echoes are at a fixed shortest TE in the third window like (b). In addition, three pulse sequences mentioned above are all under the constant magnetic field gradients, while (d) is the 3D pulse sequence with the PFG. The gradient is applied in two short gradient pulses, which are of time width δ and separation Δ. The sum of δ and Δ is referred to as the diffusion time. The following CPMG sequence is same to the pulse sequences above. Therefore, the kernel function K_3 of these four acquisition methods can be expressed as:

$$k_3(t,TE,D)=\exp(-\gamma^2G^2TE^2Dt/12) \quad (4)$$

$$k_3(t,NE_1,D)=\exp(-\gamma^2G^2{t_0}^3D/12NE_1) \quad (5)$$

$$k_3(t,TE_1,D)=\exp(-\gamma^2G^2{TE_1}^3D/6) \quad (6)$$

$$k_3(t,G,D)=\exp(-\gamma^2G^2\delta^2(\Delta-\frac{\delta}{3})D) \quad (7)$$

Note that detection time t begins at CPMG pulse sequence, that is to say, the diffusion information is encoded in the initial magnetization amplitude in the third window in (b), (c) and (d). NE1 in Eq. (5) is the number of echo in the second window based on the echo spacing (TE_1).

It shows that the 3D pulse sequences are simple combinations of 2D pulse sequences or regular CPMG pulse sequence. Meanwhile, according to the introduction in the first section, the inversion scheme of 3D NMR is commonly based on dimensionality reduction or direct one-step inversion that integrates the tangled kernels as a single kernel. Therefore, the main problems for 3D NMR in detecting the cores with complex relaxation components are as follows: (1) The range of G, the static external magnetic field gradients, is narrow in 3D pulse sequence because of the restriction of instrument and influence on diffusion-free relaxation informa-

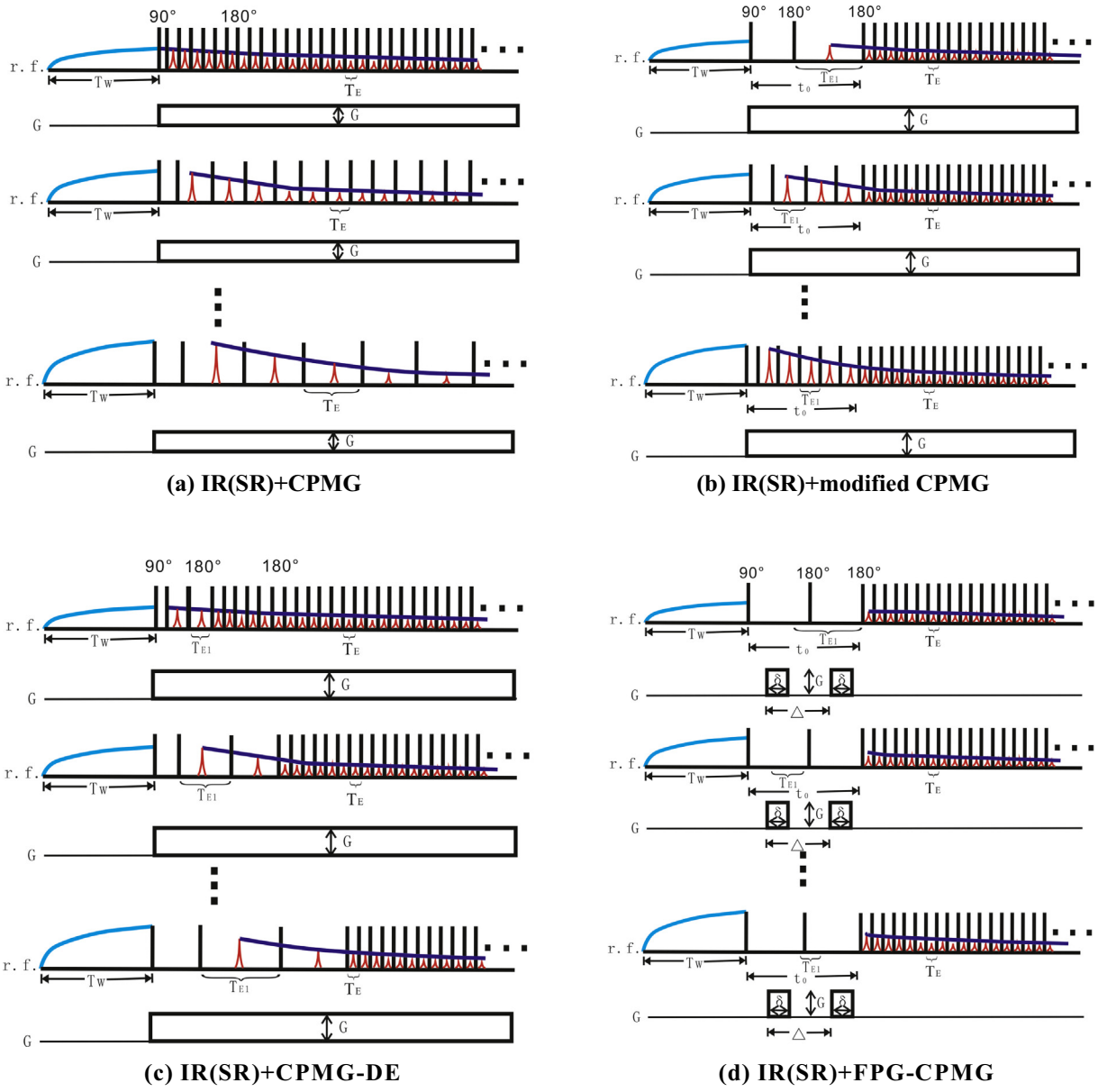

Fig. 1. Schematic diagrams of four conventional T_1-T_2-D pulse sequences.

tion. Thus, "tail" is often showed in NMR map and affects the interpretation because of the low capability in diffusion editing. Additionally, for the pulse sequence (a), the increasing TE will sharply reduce the number of echoes, which losses the effect information and limits the accuracy of inversion. (2) The diffusion relaxation is not considered in CPMG window in 3D pulse sequences based on modified CPMG and CPMG-DE. Actually, despite of the minimum TE and relatively low G, the diffusion relaxation cannot be completely ignored. Additionally, despite very few echo spins can still be detected in the diffusion-editing window, the T_2 relaxation are not considered in inversion algorithm mainly because the complexity of inversion and the lack of sufficient information. It is obviously a limitation because fast relaxation components could have been completely decayed in this period time. (3) Due to the high value of PFG, the measuring range of D in 3D pulse sequence based on PFG is large. However, magnetization decay data cannot be acquired in the diffusion-editing window, leading to the low resolution of the fast relaxation components.

Therefore, new design should have two main advantages: (1) New pulse sequence can balance the resolution of diffusion coefficient and transverse relaxation. It can also acquire adequate magnetization decay data of fast relaxation components. (2) New inversion method should take more account of the fast relaxation components from algorithm scheme and data format.

3. Method

3.1. Tri-window pulse sequence

We propose a novel 3D pulse sequence with three editing windows (Fig. 2), based on the T_2-D pulse sequence we proposed before [53]. IR is used to encode T_1 in the first window because the dynamic range of magnetization is twice larger than that of SR. Then pulse field gradient is exerted in the second window, whose parameters such as duration time and gradient value can be adjusted to satisfy different experimental subjects. The greatest advantage of this diffusion editing method is that T_2 and D are simultaneously encoded in this second window, then sufficient and effective decay information of fast relaxation components could be acquired. The diffusion effect is positively correlated with

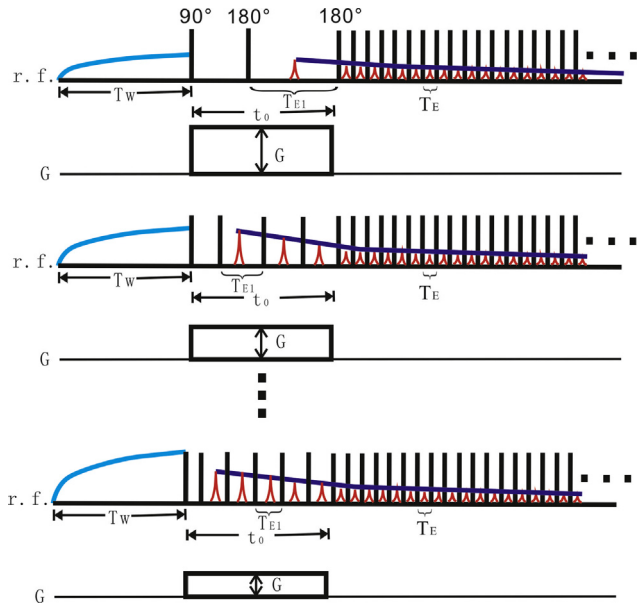

Fig. 2. Schematic diagram of new 3D pulse sequence.

the gradient value and TE, thus appropriate combination of PFG and TE in the second window is critical to the detection and separation of the components with complex diffusion relaxation time and short transverse relaxation time. The third window is the regular CPMG pulse sequence with the shortest TE. Note that there is no field gradient in this window so that the influence of diffusion can be totally ignored.

Three kernels characterizing the time evolution of magnetization can be expressed as:

$$k_1 = (1 - 2\exp(-TW_s/T_{1r})) \tag{8}$$

$$k_{2,1} = \exp\left(-\frac{i\gamma^2 G_s{}^2 t_0{}^3 D_p}{12 NE_{1s}{}^3}\right); \quad k_{2,2} = \exp\left(-\frac{\gamma^2 G_s{}^2 t_0{}^3 D_p}{12 NE_{1s}{}^2}\right) \tag{9}$$

$$k_{3,1} = \exp\left(-\frac{i \cdot t_0}{NE_{1s} \cdot T_{2j}}\right); \quad k_{3,2} = \exp\left[-\frac{t_0 + (i - NE_{1s}) \cdot TE_2}{T_{2j}}\right] \tag{10}$$

where $k_{2,1}$ and $k_{3,1}$ represent the kernel functions in the second window while $k_{2,2}$ and $k_{3,2}$ represent the kernel functions in the third window. When Eq. (1) is discretized, the magnetization decay data can be written as:

$$b_{is} = \begin{cases} \sum_{r=1}^{l}\sum_{j=1}^{m}\sum_{p=1}^{n} f(T_{1r}, T_{2j}, D_p) k_1 k_{2,1} k_{3,1} & i = 1, 2 \ldots NE_{1s}, NE_{1s} \cdot TE_{1s} = t_0 \quad \text{(a)} \\ \sum_{r=1}^{l}\sum_{j=1}^{m}\sum_{p=1}^{n} f(T_{1r}, T_{2j}, D_p) k_1 k_{2,2} k_{3,2} & i = NE_{1s}+1, NE_{1s}+2, \ldots, NE_{1s}+NE_2 \quad \text{(b)} \end{cases} \tag{11}$$

where b_{is} denotes the amplitude of the ith spin echo in the sth echo train. The wait time in the first window is TW_s, the number of echo in the second window is NE_{1s} and the pulsed field gradient is G_s. The number of the echo trains is M; $f(T_{1r}, T_{2j}, D_p)$ denotes the proton density distribution function corresponding to the transverse relaxation time T_{2j}, longitudinal relaxation time T_{1r} and diffusion coefficient D_p; t_0 is the duration time of the second window and the echo spacing is $TE_{1s}(TE_{1s} = t_0/NE_{1s})$; TE_2 is the smallest echo spacing the NMR core analyzer allowed in the third window. NE_2 is the number of echo in the third window and unchanged in all echo trains in our design. l, m, n are the numbers of T1, T_2 and D values or bins. Eq. (11a) is the integral equation for the second window while Eq. (11b) for the third window. In addition, when $i > NE_{1s}$, k_1, $k_{2,2}$ and $k_{3,2}$ are separate and uncoupled. While when $i < NE_{1s}$, $k_{2,1}$ and $k_{3,1}$ are tangled because of the parameter i. Finally, decay datasets can be acquired by varying the TW in the first window, TE and G in the second window.

In addition, in order to obtain high-resolution decay information and inversion results, more detailed analysis on acquisition parameters are required before simulation and experiment. For example, t_0, NE_{1s} and G_s are key parameters in diffusion editing window, the detectability of diffusion coefficient is proportional to t_0 and G_s, while inversely to NE_{1s}. In addition, TW_s, NE_2, TE_2, M and the number of scans are also the influence factors of the decay spectrums, controlling the acquisition data resolution and SNR. Therefore the acquisition parameters should be considered carefully.

3.2. Novel inversion algorithm

According to the above introduction, two decay datasets are acquired in the new pulse sequence. Although we could obtain the inversion 3D NMR spectrums both from two datasets, the difference between two inversion results should be noted because decay data in the second window mainly represents the signal of fast relaxation components while decay data in the third window mainly represents the signal of slow relaxation components. Obviously, a more exact 3D NMR spectrum could be obtained by combining these two inversion results. Thus, we consider two datasets at the same time and propose a joint inversion algorithm (Fig. 3).

For the decay function in the third window (Eq. (11b)), k_1, $k_{2,2}$ and $k_{3,2}$ are separate and uncoupled. Considering the large size of $k_{3,2}$, whose size is $NE_2 \times m$, we combine the k_1 and $k_{2,2}$ as $k_{1,2}$. Meanwhile, f is reshaped as f_{T_1D}, so that the 3D inversion problem can be simplified as a 2D inversion problem. For simplicity, the size of each parameter is listed in the following bracket.

$$k_{12}(M \times (l \times n)) = combine(k_1(M \times l), k_{2,2}(M \times n)) \tag{12}$$

$$f_{T_1D}(m \times (l \times n)) = reshape(f(l \times m \times n)) \tag{13}$$

$$b_2(NE_2 \times M) = k_{32}(NE_2 \times m) \cdot f_{T_1D}(m \times (l \times n)) \cdot k_{12}{}'(M \times (l \times n)) + \varepsilon_2 \tag{14}$$

To obtain the solution f_{T_1D}, 2D inversion method can be used to solve this least squares problem:

$$\arg\min_{f \geqslant 0} \| b_2 - k_{32} f_{T_1D} k'_{12} \|^2 \tag{15}$$

In order to accelerate the calculation, data are compressed by using SVD of the kernels matrix [31]. SVD is implemented for $k_{3,2}$ and $k_{1,2}$ separately. $S_{3,2}$ and $S_{1,2}$ are diagonal matrixes with the singular values in decreasing order along the diagonals, the size of which are determined by the number of truncated singular values according to SNR.

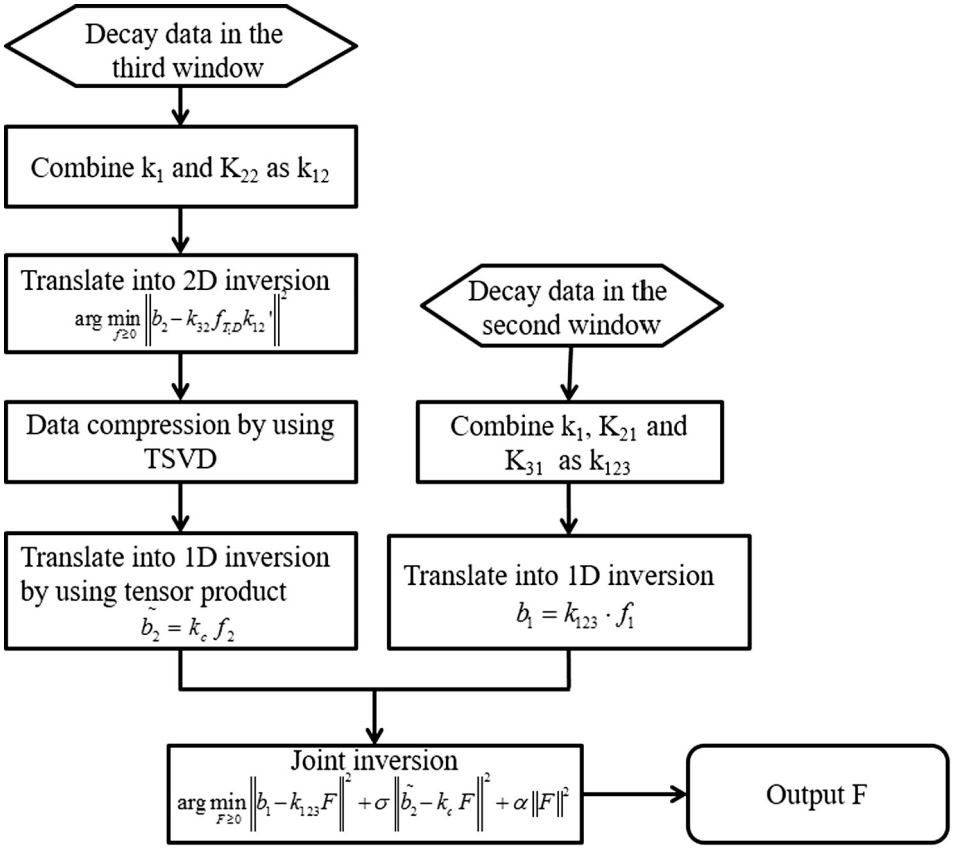

Fig. 3. The joint inversion scheme.

$$k_{32} = U_{32}S_{32}V_{32}^T \tag{16}$$

$$k_{12} = U_{12}S_{12}V_{12}^T \tag{17}$$

Ignoring the noise, Eq. (14) can be reorganized by the truncated matrices:

$$b_2 = U_{32}S_{32}V_{32}^T f_{T_1D}(U_{12}S_{12}V_{12}^T)^T = U_{32}S_{32}V_{32}^T f_{T_1D}V_{12}S_{12}^T U_{12}^T \tag{18}$$

Assuming the truncated matrices $\tilde{k}_{32} = S_{32}V_{32}^T$ and $\tilde{k}_{12} = S_{12}V_{12}^T$, the truncated data can be expressed as:

$$\tilde{b}_2 = U_{32}^T b_2 U_{12} = S_{32}V_{32}^T f_{T_1D}V_{12}S_{12}^T = \tilde{k}_{32} f_{T_1D} \tilde{k}_{12}^T \tag{19}$$

$$k_c = \tilde{k}_{32} \otimes \tilde{k}_{12} \tag{20}$$

$$\tilde{b}_2 = k_c f_2 \tag{21}$$

where vectors $\tilde{b}_2$ and f_2 are obtained by lexicographically ordering matrices b_2 and $\tilde{f}_{T_1D}$, respectively. Finally, the 3D NMR inversion problem is simplified as a 1D NMR inversion problem gradually.

For the decay function in the second window (Eq. 11a), $k_{2,1}$ and $k_{3,1}$ are tangled and coupled. Considering the small size of k_1, $k_{2,1}$ and $k_{3,1}$ since the number of echoes in the second window is small, the problem can be cast in a one-step inversion problem by integrating three kernels as a single kernel:

$$k_{123}\left(\sum_{s=1}^{M} NE_{1s} \times (l \times m \times n)\right) = combine\left(k_1(M \times l), k_{2,1}\left(\sum_{s=1}^{M} NE_{1s} \times n\right), k_{3,1}\left(\sum_{s=1}^{M} NE_{1s}s \times m\right)\right) \tag{22}$$

$$f_1((l \times m \times n) \times 1) = reshape(f(l \times m \times n)) \tag{23}$$

$$b_1\left(\sum_{s=1}^{M} NE_{1s} \times 1\right) = k_{123}\left(\sum_{s=1}^{M} NE_{1s} \times (l \times m \times n)\right) \cdot f_1((l \times m \times n) \times 1) + \varepsilon_1 \tag{24}$$

where vector f_1 is obtained by lexicographically ordering matrix f. Finally, data processing in the second window is also simplified as a 1D NMR inversion problem. Obviously, although obtained from different datasets, f_1 is equal to f_2. Thus, the joint inversion can be translated to a Tikhonov regularization problem. The fundamental of this kind "composite-data processing" is that two inversion problems have the same solution.

$$\arg\min_{F \geqslant 0} ||b_1 - k_{123}F||^2 + \sigma||\tilde{b}_2 - k_c F||^2 + \alpha||F||^2 \tag{25}$$

where $\|\cdot\|$ denotes the Frobenius norm of a matrix is α regularization parameter, which denotes the weighting degree and should be chosen properly to balance the least-squares error and the desired smoothness. The optimal regularization parameter can be selected by many methods such as discrepancy principle (DP), generalized cross-validation (GCV), S-curve, L-curve and the slope of L-curve, but it is not the emphasis of this paper [54,55]. L-curve is used in our numerical simulation.

σ is weight parameter, which can balance the inversion results of two datasets and the inversion accuracy. Based on the different data process strategies in the second and third window, the data size of b_1 is extremely larger than $\tilde{b}_2$. Therefore, the joint inversion should consider the data size and balance the inversion error. The choice of σ is based on the compression ratio and the difference of the data size of b_1 and $\tilde{b}_2$. In addition, to obtain the non-negative constraint of solution, the iterative solution is commonly made

by eliminating the columns of kernel matrix corresponding to the negative components in the solution or replacing them with large constants. Finally, continuous NMR spectrum can be obtained through joint inversion by inversing these two datasets simultaneously.

4. Numerical simulation

We present numerical simulations to validate the new data acquisition method and inversion algorithm. Firstly, a tight oil shale model containing four types of fluid is established by the fluid component decomposition method. The NMR properties and saturation of different components according to the typical NMR spectrums are shown in Table 1 [56–59]. Fig. 4 illustrates the simulated 3D spectrum and its correlated T_1-T_2, T_1-D and T_2-D projections, respectively. Then, 15 sets of simulated echo train of the tight oil shale model is shown in Fig. 5, which are established based on the acquisition parameters listed in Table 2. Note that the inversion recovery delay lists are logarithmically spaced with 15 entries and varied from 0.1 ms to 1000 ms. Fifteen datasets are divided into three parts according to the range of recovery time, in each part there are same permutation of the echo spacing TE1 and pulse field gradient G. Based on this design, T_2, T_1 and D could be simultaneously encoded in a few echo trains. The decay data in the second window (before 10 ms) mainly represents the signal of fast relaxation components such as bitumen, bound water and oil in the organic pores, while decay data in the third window (after 10 ms) mainly represents the signal of slow relaxation component such as oil in inorganic pores. It reveals that the decay information of fast and slow relaxation components could be acquired simultaneously by this new three dimensional pulse sequence. Fig. 6 shows the inversion results of the simulated data with the SNR of 100, 50 and 20. In our joint inversion algorithm, the number of T_1, T_2 and D bins are all 30, so that the dimension of inversed 3D spectrum is $30 \times 30 \times 30$. It reveals that the inverted NMR spectrums match well with the forward model when SNR is 100 and 50. Four types of fluid could be distinguished clearly in three projections although there are "trailing" in T_2 axis and D axis. However, unsatisfied result is observed when SNR is lower than 20, the signals of bitumen and bound water are overlapped in T_1-T_2 spectrum, while the signals of bitumen and oil in organic pores are overlapped in T_2-D spectrum. However, different fluids can be effectively distinguished in T_1-D spectrum. It is obviously one of the advantages of 3D NMR technology since T_1-D spectrum can not be obtained directly by any method. We calculated the relative error based on Eq. (26) to evaluate the inversion results:

$$R = \frac{||X_{mod} - X_{inv}||}{||X_{mod}||} \times 100\% \quad (26)$$

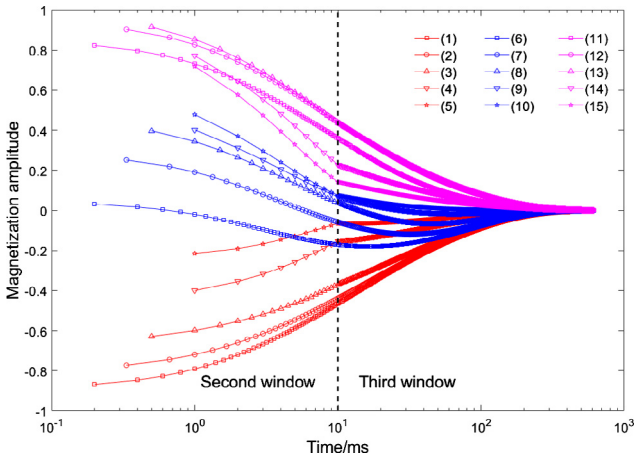

Fig. 5. Simulated echo trains of tight oil shale model.

Table 2
Acquisition parameters of tight oil shale model.

s	Tw (ms)	G (T/m)	NE1	TE1 (ms)
1	0.10	0.5	50	0.2
2	0.19	2.25	30	0.33
3	0.37	4	20	0.5
4	0.72	5.75	10	1
5	1.39	7.5	10	1
6	2.68	0.5	50	0.2
7	5.18	2.25	30	0.33
8	10.00	4	20	0.5
9	19.31	5.75	10	1
10	37.28	7.5	10	1
11	71.97	0.5	50	0.2
12	138.95	2.25	30	0.33
13	268.27	4	20	0.5
14	517.95	5.75	10	1
15	1000.00	7.5	10	1
T_0 = 10 ms	TE_2 = 0.2 ms	NE_2 = 3000	$\gamma = 2.675 \times 10^8$ rad/s/T	

Table 1
NMR properties and saturation of components in tight oil shale model.

Components	T_1 (ms)	T_2 (ms)	D (cm^2/s)	Saturation (%)
Bound water	2	1.5	4×10^{-5}	15
Bitumen	5	0.5	1×10^{-6}	15
Oil in OP	15	3	4×10^{-6}	40
Oil in IP	80	50	4×10^{-6}	30

OP – organic porosity; IP – inorganic porosity.

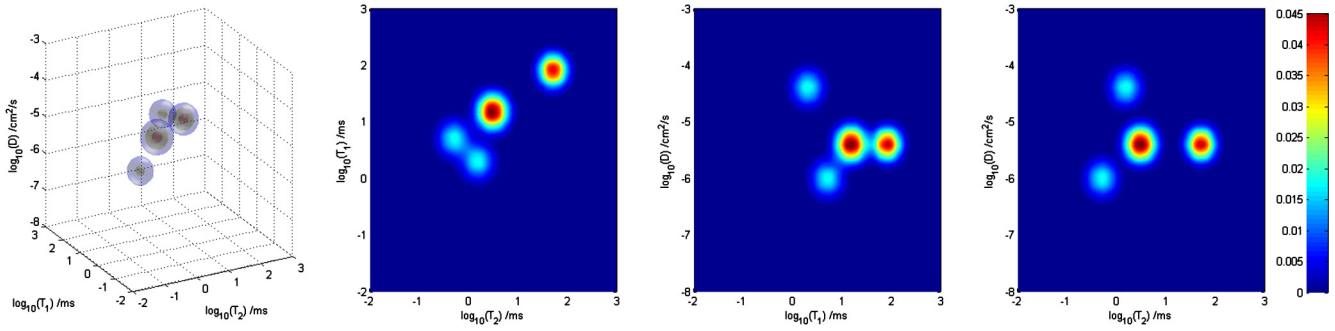

Fig. 4. Simulated spectrums of tight oil shale.

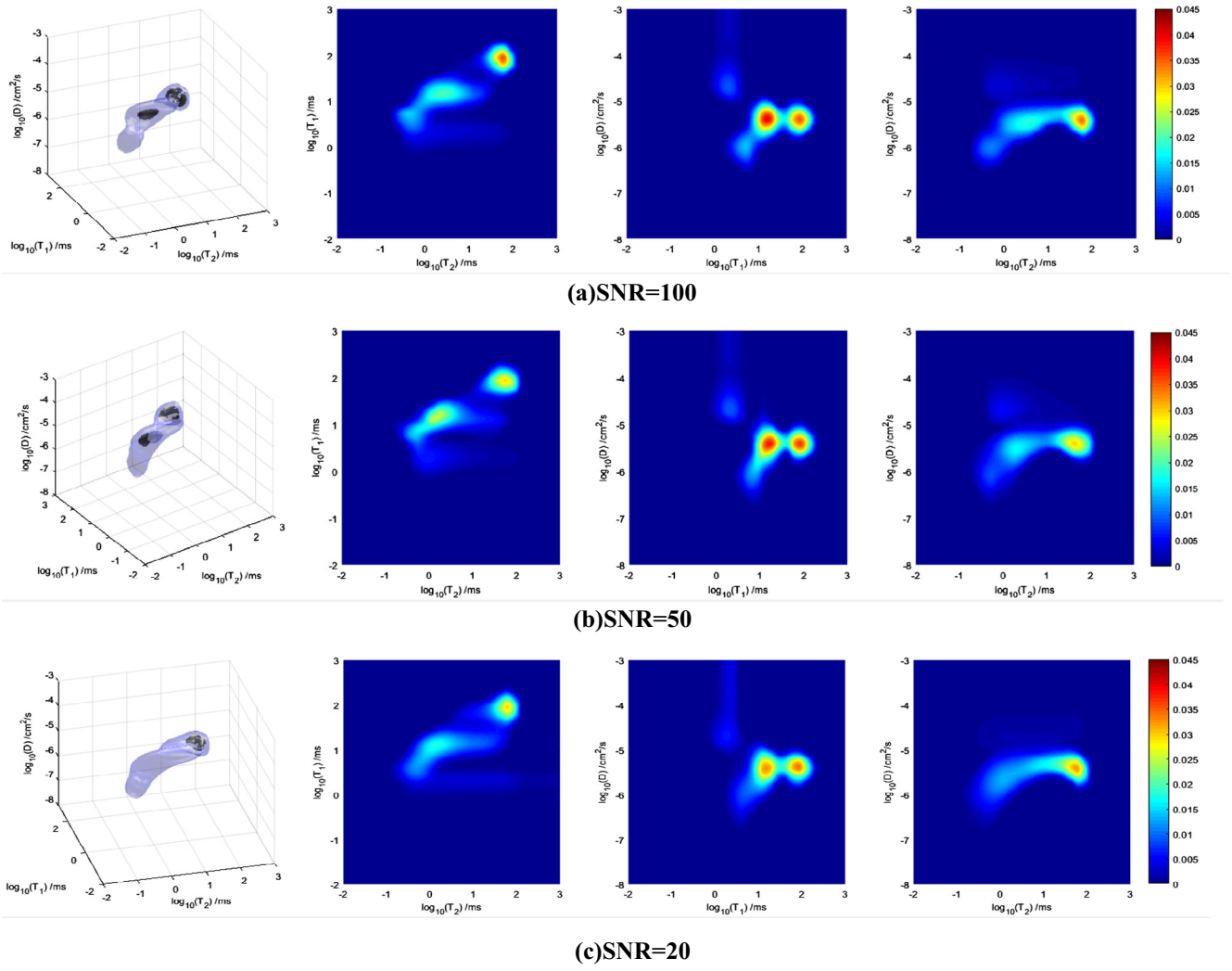

Fig. 6. Inversion results of tight oil shale with different SNRs.

Table 3
Comparison of R between the inverted and simulated spectrum.

SNR	100	50	20
R	0.4146	0.6037	0.9712

where X_{mod} is simulated data and X_{inv} is inverted data. Table 3 lists comparison of R between inverted and simulated spectrum. After the processing of joint regularization inversion, R keeps at low levels with different SNRs. It reveals that the joint inversion algorithm is of good performance in data with SNR higher than 20.

5. Conclusions

In this work, we present a new pulse sequence and inversion algorithm of 3D NMR to acquire the decay data of fast and slow relaxation components simulantously and optimize the data processing. The conclusions are summarized as follows:

(1) The new pulse sequence, which includes three windows, is superior to conventional acquisition method since two datasets are acquired, representing the magnetization decay information of fast and slow relaxation components respectively.
(2) The stable solution of the ill-posed problem can be obtained through the joint inversion scheme since two datasets are inversed simultaneously.
(3) The proposed pulse sequence and inversion algorithm are of great importance for NMR experiment and well logging, especially in the identification of complex relaxation components in unconventional resources.

However, the novel pulse sequence has not been implemented in actual instrument at current stage. Much work should be done to reach the aim of industry application.

Acknowledgements

This work was supported by the Fundamental Research Funds for the Central Universities, China (18CX06025A,19CX02006A), National Science and Technology Major Project, China (2017ZX05039-002, 2017ZX05072-002) and the Laboratory for Marine Mineral Resources, Qingdao National Laboratory for Marine Science and Technology (MMRZZ201805).

References

[1] G.R. Coates, L.Z. Xiao, M.G. Prammer, NMR Logging Principles and Applications, Gulf Publishing Company, Texas, USA, 1999.

[2] K.J. Dunn, D.J. Bergman, G.A. Latorraca, Nuclear Magnetic Resonance Petrophysical and Logging Application, Elsevier Science Ltd., 2002.
[3] J. Mitchell, M.D. Hürlimann, E.J. Fordham, A rapid measurement of T1/T2: the DECPMG sequence, J. Magn. Reson. 200 (2) (2009) 198–206.
[4] F. Deng, L. Xiao, G. Liao, A new approach of two-dimensional the NMR relaxation measurement in flowing fluid, Appl. Magn. Reson. 45 (2) (2014) 179–192.
[5] F. Deng, L. Xiao, W. Chen, Rapid determination of fluid viscosity using low-field two-dimensional NMR, J. Magn. Reson. 247 (2014) 1–8.
[6] W. Chen, L. Xiao, Y. Zhang, Rapid T1–T2 measurement using drive equilibrium pulse sequence, Appl. Magn. Reson. 47 (10) (2016) 1159–1169.
[7] E.O. Stejskal, J.E. Tanner, Spin diffusion measurements: spin echoes in the presence of a time-dependent field gradient, J. Chem. Phys. 42 (1) (1965) 288–292.
[8] E.O. Stejskal, Use of spin echoes in a pulsed magnetic-field gradient to study anisotropic, restricted diffusion and flow, J. Chem. Phys. 43 (10) (1965) 3597–3603.
[9] R.F. Karlicek, I.J. Lowe, A modified pulsed gradient technique for measuring diffusion in the presence of large background gradients, J. Magn. Reson. (1969) 37 (1) (1980) 75–91.
[10] R.M. Cotts, M.J.R. Hoch, T. Sun, Pulsed field gradient stimulated echo methods for improved NMR diffusion measurements in heterogeneous systems, J. Magn. Reson. (1969) 83 (2) (1989) 252–266.
[11] L.L. Latour, L.M. Li, C.H. Sotak, Improved PFG stimulated-echo method for the measurement of diffusion in inhomogeneous fields, J. Magn. Reson., Ser. B 101 (1) (1993) 72–77.
[12] D. Vandusschoten, P.A. Dejager, H. Vanas, Flexible PFG NMR desensitized for susceptibility artifacts, using the PFG multiple-spin-echo sequence, J. Magn. Reson., Ser. A 112 (2) (1995) 237–240.
[13] R.W. Mair, D.G. Cory, S. Peled, et al., Pulsed-field-gradient measurements of time-dependent gas diffusion, J. Magn. Reson. 135 (2) (1998) 478–486.
[14] M.W. Hunter, A.N. Jackson, P.T. Callaghan, PGSE NMR measurement of the non-local dispersion tensor for flow in porous media, J. Magn. Reson. 204 (1) (2010) 11–20.
[15] G. Goelman, M.G. Prammer, The CPMG pulse sequence in strong magnetic field gradients with applications to oil-well logging, J. Magn. Reson., Ser A 113 (1) (1995) 11–18.
[16] M.D. Hürlimann, L. Venkataramanan, Quantitative measurement of two-dimensional distribution functions of diffusion and relaxation in grossly inhomogeneous fields, J. Magn. Reson. 157 (1) (2002) 31–42.
[17] M.D. Hürlimann, L. Venkataramanan, C. Flaum, Diffusion-editing: new NMR measurement of saturation and pore geometry, SPWLA 43rd Annual Logging Symposium. Society of Petrophysicists and Well-Log Analysts, 2002.
[18] B. Sun, K.J. Dunn, Probing the internal field gradients of porous media, Phys. Rev. E 65 (5) (2002).
[19] Y.-Q. Song, Magnetic Resonance of porous media (MRPM): a perspective, J. Magn. Reson. 229 (2013) 12–24.
[20] G.C. Borgia, R.J.S. Brown, P. Fantazzini, Uniform-penalty inversion of multiexponential decay data, J. Magn. Reson. 132 (1) (1998) 65–77.
[21] J.P. Butler, J.A. Reeds, S.V. Dawson, Estimating solutions of the first kind integral equations with nonnegative constraints and optimal smoothing.SIAM, J. Numer. Anal. 18 (1981) 381–382.
[22] B. Sun, K.-J. Dunn, Methods and limitations of NMR data inversion for fluid typing, J. Magn. Reson. 169 (1) (2004) 118–128.
[23] Z. Wang, L. Xiao, T. Liu, New inversion method with multi-exponent and its application, Sci. China. (Series G) 33 (2003) 323–332 (in Chinese).
[24] B. Sun, In situ fluid typing and quantification with 1D and 2D NMR logging, Magn. Reson. Imaging. 25 (4) (2007) 521–524.
[25] M. Tan, Y. Shi, W. Zhao, G. Xie, A joint inversion of NMR dual-TW logging data and fluid typing, Chin. J. Geophys. 51 (5) (2008) 4053–4063.
[26] O. Mohnke, U. Yaramanci, Smooth and block inversion of surface NMR amplitudes and decay times using simulated annealing, J. Appl. Geo. 50 (1–2) (2002) 163–177.
[27] K. Pan, H. Chen, Y. Tan, Multi-exponential inversion of T2 spectrum in NMR based on differential evolution algorithm, Chin. Phys. Soc. 57 (2008) 5956–5961 (in Chinese).
[28] M. Prange, Y.-Q. Song, Quantifying uncertainty in NMR T2 spectra using Monte Carlo inversion, J. Magn. Reson. 196 (1) (2009) 54–60.
[29] X. Li, L. Kong, J. Cheng, L. Wu, The study of NMR relaxation time spectra multi-exponential inversion based on Lloyd-Max optimal quantization, J. Geophys. Eng. 12 (1) (2015) 144–153.
[30] D. Medellín, V.R. Ravi, C. Torres-Verdín, Multidimensional NMR inversion without Kronecker products: multilinear inversion, J. Magn. Reson. 269 (2016) 24–35.
[31] L. Venkataramanan, Y.Q. Song, M.D. Hurlimann, Solving Fredholm integrals of the first kind with tensor product structure in 2 and 2.5 dimensions, IEEE Trans. Signal Process. 50 (5) (2002) 1017–1026.
[32] M.D. Hürlimann, L. Venkataramanan, Quantitative measurement of two-dimensional distribution functions of diffusion and relaxation in grossly inhomogeneous fields, J. Magn. Reson. 157 (1) (2002) 31–42.
[33] Y.-Q. Song, L. Venkataramanan, M.D. Hurlimann, M. Flaum, P. Frulla, C. Straley, T1–T2 correlation spectra obtained using a fast two-dimensional Laplace inversion, J. Magn. Reson. 154 (2) (2002) 261–268.
[34] G. Su, X. Zhou, L. Wang, An inversion method of 2D NMR relaxation spectra in low fields based on LSQR and L-curve, J. Magn. Reson. 265 (2016) 146–152.
[35] A. Guillen, A. Legchenko, Inversion of surface nuclear magnetic resonance data by an adapted Monte Carlo method applied to water resource characterization, J. Appl. Geophys. 50 (1) (2002) 193–205.
[36] V. Bortolotti, R.J.S. Brown, P. Fantazzini, Uniform Penalty inversion of two-dimensional NMR relaxation data, Inverse Prob. 33 (1) (2016).
[37] V. Bortolotti, R.J.S. Brown, P. Fantazzini, I2DUPEN: improved 2DUPEN algorithm for inversion of two-dimensional NMR data, Micropor. Mesopor. Mater. (2017).
[38] E. Chouzenoux, S. Moussaoui, J. Idier, Efficient maximum entropy reconstruction of nuclear magnetic resonance T1–T2 spectra, IEEE Trans. Signal Process. 58 (12) (2010) 6040–6051.
[39] Q. Meng, H. Liu, J. Wang, A critical review on fundamental mechanisms of spontaneous imbibition and the impact of boundary condition, fluid viscosity and wettability, Adv. Geo-energ. Res. 1 (1) (2017) 1–17, https://doi.org/10.26804/ager.2017.01.01.
[40] L. Chen, Z. Jiang, K. Liu, Quantitative characterization of micropore structure for organic-rich Lower Silurian shale in the Upper Yangtze Platform, South China: implications for shale gas adsorption capacity, Adv. Geo-energ. Res. 1 (2) (2017) 112–123, https://doi.org/10.26804/ager.2017.02.07.
[41] H. Sidiq, B. Amin, T. Kennaird, The study of relative permeability and residual gas saturation at high pressures and high temperatures, Adv. Geo-energ. Res. 1 (1) (2017) 64–68, https://doi.org/10.26804/ager.2017.01.06.
[42] J. Li, T. Yu, X. Liang, Insights on the gas permeability change in porous shale, Adv. Geo-energ. Res. 1 (2) (2017) 69–73, https://doi.org/10.26804/ager.2017.02.01.
[43] Z.F. Zhang, L.Z. Xiao, H.B. Liu, A fast three-dimensional protocol for low-field Laplace NMR in porous media, Appl. Magn. Reson. 44 (7) (2013) 849–857.
[44] B. Sun, K.J. Dunn, A global inversion method for multi-dimensional NMR logging, J. Magn. Reson. 172 (1) (2005) 152–160.
[45] M. Tan, P. Wang, K. Mao, Comparative study of inversion methods of three-dimensional NMR and sensitivity to fluids, J. Appl. Geophys. 103 (2014) 12–30.
[46] Z.F. Zhang, L.Z. Xiao, H.B. Liu, A fast three-dimensional protocol for low-field Laplace NMR in porous media, Appl. Magn. Reson. 44 (7) (2013) 849–857.
[47] R.H. Xie, L.Z. Xiao, J.J. Liu, A method for multiple echo trains jointing inversion of NMR relaxation measurements, Chin. J. Geophys. 52 (6) (2009) 1342–1349.
[48] S. Chen, W. Shao, R. Balliet, New approaches of 3D nuclear magnetic resonance inversion for improving fluid typing, Interpretation 4 (2) (2016) SF67-SF79.
[49] D. Medellín, V.R. Ravi, C. Torres-Verdín, Multidimensional NMR inversion without Kronecker products: multilinear inversion, J. Magn. Reson. 269 (2016) 24–35.
[50] Z. Zhang, L. Xiao, G. Liao, Evaluation of the fast inverse Laplace transform for three-dimensional NMR distribution functions, Appl. Magn. Reson. 44 (11) (2013) 1335–1343.
[51] C.H. Arns, K.E. Washburn, P.T. Callaghan, Multidimensional NMR inverse Laplace spectroscopy in petrophysics1, Petrophysics 48 (05) (2007).
[52] L. Xiao, H. Liu, F. Deng, Probing internal gradients dependence in sandstones with multi-dimensional NMR, Micropor. Mesopor. Mater. 178 (2013) 90–93.
[53] F. Yi-Ren, W. Fei, L. Hu, A modified design of pulse sequence and inversion method for DT-2 two-dimensional NMR, Acta Phys. Sin. 64 (9) (2015).
[54] M. Tan, Y. Zou, C. Zhou, A new inversion method for (T2, D) 2D NMR logging and fluid typing, Comput. Geosci. 51 (2013) 366–380.
[55] Y.L. Zou, R.H. Xie, A. Arad, Numerical estimation of choice of the regularization parameter for NMR T2 inversion, Pet. Sci. 13 (2) (2016) 237–246.
[56] R. Kausik, K. Fellah, E. Rylander, NMR petrophysics for tight oil shale enabled by core resaturation, International Symposium of the Society of Core Analysts, 2014, p. 3.
[57] R. Kausik, K. Fellah, E. Rylander, NMR relaxometry in shale and implications for logging, Petrophysics 57 (04) (2016) 339–350.
[58] R. Kausik, C.C. Minh, L. Zielinski, Characterization of gas dynamics in kerogen nanopores by NMR. SPE Annual Technical Conference and Exhibition, Society of Petroleum Engineers, Denver, CO, 2011, p. 30.
[59] C. Cao Minh, S.F. Crary, L. Zielinski, 2D-NMR applications in unconventional reservoirs. SPE Canadian Unconventional Resources Conference, Society of Petroleum Engineers, 2012.